Precision Measurement of Phonon-Polaritonic Near-Field Energy Transfer between Macroscale Planar Structures Under Large Thermal Gradients

Mohammad Ghashami, Hongyao Geng, Taehoon Kim, Nicholas Iacopino, Sung Kwon Cho, and Keunhan Park

Phys. Rev. Lett. **120**, 175901 — Published 26 April 2018

DOI: 10.1103/PhysRevLett.120.175901

Precision Measurement of Phonon-Polaritonic Near-Field Energy Transfer between Macroscale Planar Structures Under Large Thermal Gradients

Mohammad Ghashami,[1] Hongyao Geng,[2] Taehoon Kim,[1] Nicholas Iacopino,[1] Sung Kwon Cho,[2] and Keunhan Park[1,*]

[1] *Department of Mechanical Engineering, University of Utah, Salt Lake City, Utah 84112, United States.*
[2] *Department of Mechanical Engineering & Materials Science, University of Pittsburgh, Pittsburgh, PA 15261, United States.*

Despite its strong potentials in emerging energy applications, near-field thermal radiation between large planar structures has not been fully explored in experiments. Particularly, it is extremely challenging to control a subwavelength gap distance with good parallelism under large thermal gradients. This article reports the precision measurement of near-field radiative energy transfer between two macroscale single-crystalline quartz plates that support surface phonon polaritons. Our measurement scheme allows the precise control of a gap distance down to 200 nm in a highly reproducible manner for a surface area of 5×5 mm^2. We have measured near-field thermal radiation as a function of the gap distance for a broad range of thermal gradients up to ∼156 K, observing more than 40 times enhancement of thermal radiation compared to the blackbody limit. By comparing with theoretical prediction based on fluctuational electrodynamics, we demonstrate that such remarkable enhancement is owing to phonon-polaritonic energy transfer across a nanoscale vacuum gap.

PACS numbers:

When two objects are separated by a nanoscale vacuum gap, thermal radiation can exceed the blackbody limit by several orders of magnitude due to photon tunneling of thermal evanescent electromagnetic (EM) waves, along with other near-field effects such as interferences and surface polaritons [1]. Such remarkable enhancement of thermal radiation can be beneficially used in many energy applications, including thermophotovoltaic [2–8] and thermionic [9] solid-state heat engines, thermal extraction [10], thermotronics [11–15], and dynamic thermal modulation [16]. However, experimental demonstration of such emerging energy applications has not been fully explored to date due to technical difficulties in precisely measuring near-field thermal radiation between large planar structures under a substantial temperature difference. Although several experimental investigations have been conducted in the tip-plane [17–20] and sphere-plane [21–28] configurations, they do not meet the large-area requirement for energy applications.

The first attempts to measure near-field thermal radiation between parallel plates date back to the late 1960s. Cravalho *et al.* [29], Domoto *et al.* [30], and Hargreaves [31] were among the first that observed a slight enhancement of thermal radiation between two metallic plates. However, their measurements were not convincing mainly due to the lack of capability in achieving a subwavelength vacuum gap separation. This technical difficulty has been addressed by placing micro/nano-spacers between planar structures as a practical and cost-effective way to achieve a subwavelength gap spacing between large plates [2, 16, 32–37]. However, undesired heat conduction through spacer-plate contacts prevents a direct measurement of near-field thermal radiation, often necessitating tedious post-processing to exclude the heat conduction contribution from the measurement. Another challenge of the micro/nano-spacer scheme is the incapability of precision gap control between plates. Only limited degree of gap controllability has been demonstrated by mechanically adjusting the gap spacing formed by spacers [16, 33–36] or repeating the measurement for different spacer sizes [37]. Recently, St-Gelais *et al.* [38, 39] measured near-field thermal radiation for a broad range of gap distances from 42 nm to 1.5 μm under thermal gradients larger than 100 K using a microelectromechanical actuator platform. However, their nanobeam configuration (i.e., 400 nm×155 μm) is not appropriate for energy applications.

In this article, we report a direct and systematic measurement of near-field thermal radiation between macroscale planar structures for broad nanoscale gap distances and large thermal gradients over 100 K. To this end, a versatile near-field experimental setup has been developed based on a nanopositioning platform. Micro/nanopositioning systems have been used to facilitate the active control of nanoscale gap distances, as demonstrated in previous works [40–43]. Figure 1a shows the experimental setup that has a nanopositioner (Smarpod 110.45, SmarAct) as a thermal receiver stage. The nanopositioner is composed of three piezo-motors, providing six degrees of freedom with 1-nm translational resolutions in x-, y-, and z-directions and 1-μrad rotational resolutions in θ_x, θ_y, and θ_z directions. The total travel range in the z-direction is about 10 mm, which allows for safe sample mounting and pre-alignment procedures. To prevent overheating of the piezo-motors during experiments, a copper heat sink and a thermoelectric cooler (TEC) (VT/HP127, TE-Tech) are mounted on the nanopositioning stage. On the other hand, the thermal emitter stage is equipped with a 20×20 mm^2 ceramic heater (HT24S, Thorlabs) that can increase its tempera-

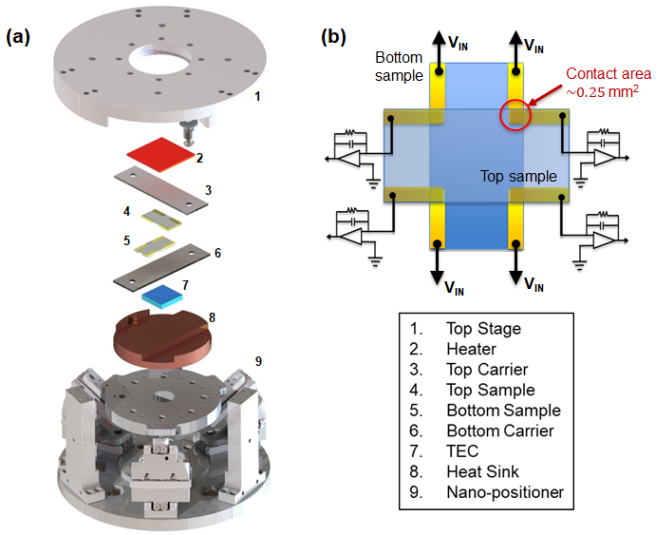

FIG. 1: (a) Schematic illustration of the near-field experimental setup, disassembled to clearly show components mounting on its two stages. (b) Schematic of pre-aligned top and bottom samples with contact sensors.

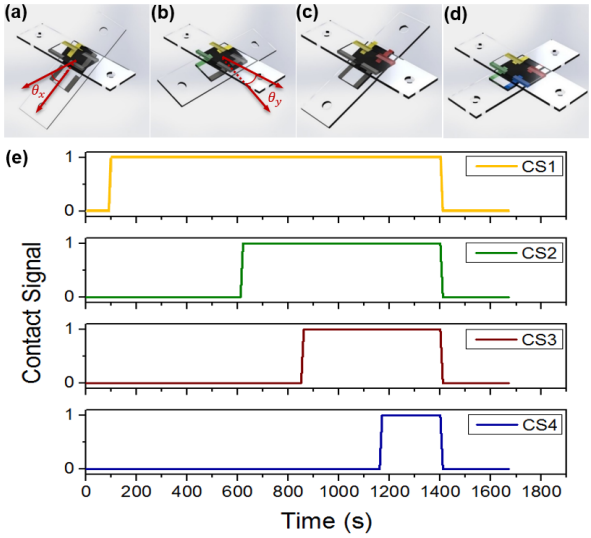

FIG. 2: (a)-(d) Sample engagement steps for parallel gap spacing: (a) bottom sample initially tilted and approached to make the first corner contact, (b) bottom sample rotates to make a two-corner contact. (c)-(d) The same procedure is repeated in the other direction until four corners can make contact. (e) Real-time monitoring of four contact signals during the sample engagement and retraction. Note that the slight inclination of the lines is just due to the small sample rate for plotting interface, not the actual electrical response.

ture up to 673 K. Once samples are prepared as described in the following paragraph, they are adhered to glass carriers (with dimensions of 30×5×0.5 mm^3) and mounted on both stages. Since the experimental setup is housed in a high-vacuum chamber, all components are assembled in a vacuum compatible manner.

Preparing samples with clean surface conditions is the key for the successful measurement of near-field thermal radiation, particularly when the gap distance is below several hundred nanometers [20]. At the same time, the sample preparation procedure should be versatile enough to allow experiments for various materials and nanostructures. In order to meet these requirements, samples are prepared with simple microfabrication processes. The schematics of sample design and initial alignment are illustrated in Fig. 1b: sample fabrication steps can be found in [44]. We selected quartz as an illustrative material due to several advantages, such as its transparency that facilitates the initial alignment step, well-established microfabrication recipes, and intrinsic flat surfaces of commercial quartz wafers. Moreover, quartz supports surface phonon polaritons at $\lambda \approx 8.5$ μm and $\lambda \approx 20.3$ μm, which are predicted to greatly enhance near-field thermal radiation [23, 51]. We design rectangular (5×15 mm^2) quartz samples, where the four corners are coated with silver (0.5×5.5 mm^2). When two samples are aligned perpendicular as shown in Fig. 1b, the overlapped quartz surface area is 5×5 mm^2 while the Ag patterns cover 0.5×0.5 mm^2 on average at each corner (or ∼1% of the total surface area). These overlapped Ag patterns are used as contact sensors, which will be discussed later. The Ag layer thickness is 10.2 ± 0.4 nm as measured with a profilometer (Tencor, P-10) for different samples in one batch: the Ag layer profiles of one illustrative sample are shown in Fig. S7 [44]. After fabrication, we applied a cleaning protocol to samples as described in [44] and sealed them in a pre-treated container, all conducted in a 100-class cleanroom. In addition, all near-field experiments were conducted in a 1000-class modular cleanroom to avoid sample contamination during experiments.

The sample engagement procedure to ensure a parallel gap spacing is depicted in Figs. 2a-d. Initially with no power supplied to the heater and TEC, the bottom sample is slightly tilted and moved up slowly (<10 nm/s) to make contact at one corner. Next step is to rotate the bottom sample around either x- or y-axis (i.e., θ_x or θ_y) until two contacts in one direction are made. The same step is repeated on the other axis to make all four corners in contact [52]. Figure 2e shows a typical sensing sequence of the four-corner contact sensors during the sample engagement procedure, where each signal (distinguished by color) indicates a contact made between two Ag pads at a specific corner. Once the four corners are in contact, two plates are expected to have a parallel gap spacing as confirmed by the concurrent signal-off from all contact sensors during slow retraction in Fig. 2e. Once the bottom stage is retracted, electric power is supplied to the ceramic heater and the TEC to obtain set-point temperatures. It should be noted that the sample heating may cause non-uniform thermal expansion of

the sample assemblies, often necessitating sample realignment to secure the four-corner contact. After the realignment procedure is completed, the bottom stage moves to a desired position while the samples temperatures are feedback-controlled. The vertical displacement of the nanopositioner (ΔZ_p) was calibrated with optical interferometry, revealing that ΔZ_p is in excellent match with the interferometrically measured displacement (ΔZ_i) as $\Delta Z_i/\Delta Z_p = 1.0014 \pm 0.0009$ [44].

As illustrated in Fig. 3a, energy balance at the top (thermal emitter) stage can be written as

$$P_H(d) = Q_R(d) + Q_{Loss} \tag{1}$$

where P_H is electric power supplied to the heater, Q_R is the radiative heat transfer rate from the top to the bottom sample across the vacuum gap d, and Q_{Loss} is heat loss to the surrounding by thermal conduction to the top stage and thermal radiation to the vacuum chamber. On the other hand, the energy balance at the bottom (thermal receiver) stage can be written as $Q_{Out} = Q_R(d) + P_{TEC}$, where Q_{Out} is heat dissipation to the heat sink and P_{TEC} is electric power supplied to the TEC. In eq 1, only Q_{Loss} is not a function of the gap distance, suggesting that Q_{Loss} should be constant at different gap distances as far as the heater maintains at the same temperature. Therefore, the near-field contribution in thermal radiation can be determined by

$$\Delta Q_R(d) = P_H(d) - P_{H,FF} \tag{2}$$

where $P_{H,FF}$ ($= Q_{FF} + Q_{Loss}$) is the heater power in the far-field regime for the same experimental condition, and Q_{FF} is far-field thermal radiation.

We measured the heater power (P_H) at different gap distances ranging from 200 nm to 1200 nm while maintaining the heater temperature (T_{Heater}) and the TEC temperature (T_{TEC}) at setpoints. In addition, $P_{H,FF}$ was measured at $d = 10$ μm, which is longer than the thermal wavelengths (i.e., $\lambda_T = \hbar c/k_B T$) at heater temperatures under consideration. It should be noted that the minimum gap distance of 200 nm was rigorously determined by repeating near-field experiments for different samples and thermal gradients. We believe that the surface bow and uneven thermal expansion of sample assemblies are the main limiting factor of the achievable gap distance in the current experimental setup [44]. In order to compare the measurements with theoretical calculations, the exact surface temperatures (i.e., T_H and T_C) should be known. Since it is challenging to directly measure T_H and T_C while the gap distance maintains at nanoscales [35, 36], we instead estimated the possible ranges of T_H and T_C (or $\Delta T = T_H - T_C$) by conducting the far-field calibration and near-field thermal circuit analysis at $d = 200$ nm [44].

Figure 3b shows the measurement of near-field thermal radiation between two quartz samples when T_H and T_C

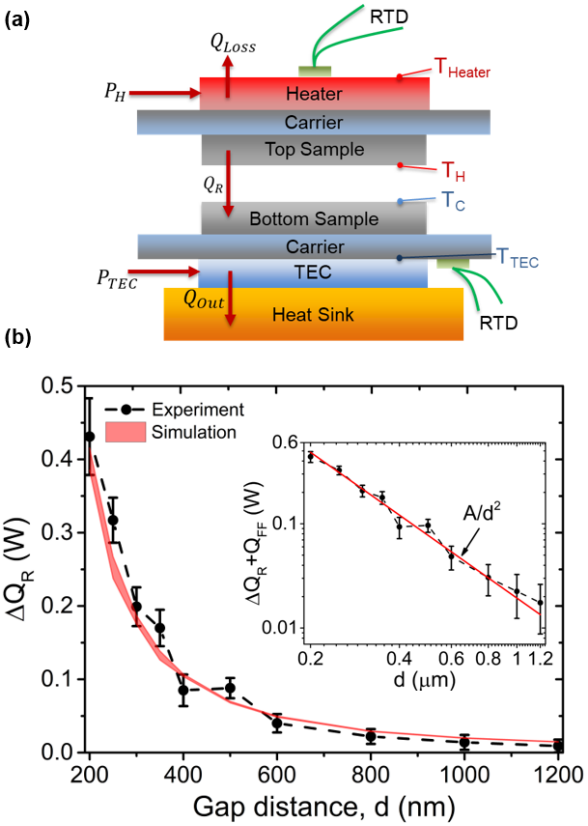

FIG. 3: (a) Measurement principle of near-field thermal radiation, where Q_R is measured at different gap distances while T_{Heater} and T_{TEC} are maintained at setpoints. (b) Near-field contribution in thermal radiation (ΔQ_R) between quartz plates as a function of gap distance when ΔT is 48±2 K (i.e., $T_H = 349 \pm 1$ K and $T_C = 301 \pm 1$ K). The red-colored band is the theoretical calculation obtained from fluctuational electrodynamics. The inset clearly shows the $1/d^2$ gap-dependence of near-field thermal radiation, which is a strong evidence of surface-mode dominant energy transfer.

are 349±1 K and 301±1 K, respectively, (or $\Delta T = 48 \pm 2$ K) under the vacuum condition of 8×10^{-7} Torr. The measurement is in excellent agreement with the calculation of near-field thermal radiation (colored band) based on the fluctuational electrodynamics [53, 54] within the measurement uncertainty estimated from five measurement data sets: the computational model is briefly described in [44]. The obtained result clearly demonstrates the significant enhancement of thermal radiation across nanoscale gap distances between quartz plates. This near-field enhancement can be better represented by defining the enhancement factor as $\eta_e = (\Delta Q_R + Q_{FF})/Q_{BB}$, where Q_{BB} is the blackbody limit at the same sample temperatures, i.e., $Q_{BB} = A_s \sigma (T_H^4 - T_C^4)$ with A_s being the sample surface area and σ is the Stefan-Boltzmann constant. If far-field thermal radiation is estimated using $Q_{FF} = \varepsilon Q_{BB}/(2 - \varepsilon)$, where $\varepsilon = 0.93$ is the total emissivity of quartz [55], Q_{FF} is approximately

8.5 mW (or ∼87% of the blackbody limit). The maximum enhancement factor ($\eta_{e,\max}$) is then estimated to be 45±3 at the gap distance of 200 nm, which is much greater than the previously reported enhancement factors between macroscale plates [33–37]. We believe that such significant near-field enhancement in our study is owing to the excitation of surface phonon polaritons on the quartz surfaces. The inset of Fig. 3b manifests the $1/d^2$ gap-dependence of the measured near-field thermal radiation, which signifies the strong contribution of surface modes (i.e., surface phonon polaritons for quartz) in near-field energy transfer [51, 56, 57]. Previous studies have revealed that the electromagnetic local density of states in the vicinity of polar materials, such as SiO_2 and SiC, exhibits a sharp peak at the excitation frequency of surface phonon polaritons, leading to the resonant radiative energy transport across the nanoscale vacuum gap [15, 43, 51, 58, 59].

Encouraged by the successful measurement in Fig. 3b, we repeated the experiment to measure ΔQ_R for different thermal gradients, i.e., $\Delta T = 19\pm1$ K ($T_H = 319.5\pm0.5$ K and $T_C = 300.5\pm0.5$ K), $\Delta T = 87\pm3$ K ($T_H = 388.5\pm1.5$ K and $T_C = 301.5\pm1.5$ K) and $\Delta T = 156\pm4$ K ($T_H = 471\pm2$ K and $T_C = 315\pm2$ K): see Fig. 4. In this figure, each ΔQ_R curve is slightly offset by 0.05 W for better presentation of the results. Figure 4 clearly demonstrates that the developed experimental platform can reliably measure near-field thermal radiation for a broad range of sample temperatures. However, there exists a slight discrepancy between the measured ΔQ_R and the calculation at $\Delta T = 156\pm4$ K, indicating a practical challenge in the precision gap control at large temperature gradients. Moreover, the cold side temperature is not easily manageable at large thermal gradient conditions. The TEC/heat sink assembly can maintain the thermal receiver temperature close to room temperature at ∼300 K while increasing the thermal emitter temperature up to $T_H = 388.5\pm1.5$ K (or $\Delta T = 87\pm3$ K). This experimental constraint is of particular importance for a near-field thermophotovoltaic (TPV) system where a TPV cell should be maintained near room temperature for its reliable performance [60]. However, at $\Delta T = 156\pm4$ K the TEC cannot maintain the thermal receiver at room temperature due to its limited cooling capacity. Therefore, the thermal emitter temperature is maintained at 471±2 K while the receiver sample is slightly heated to 315±2 K. This suggests that a better cooling scheme, either placing multi-stack TECs on a bigger heat sink or a liquid cooling stage, should be implemented to measure near-field thermal radiation for larger thermal gradients. The inset of Fig. 4 shows that the maximum enhancement factor at $d = 200$ nm, determined from the measurement and the theory, decreases as the thermal gradient (ΔT) increases. This decreasing trend is due to a smaller thermal wavelength (i.e., $\lambda_T = \hbar c/k_B T$) at higher thermal emitter temperatures, resulting in less photon tunneling across the same gap distance. From the definition of the enhancement factor, the near-field thermal radiation conductance can be expressed as $G_{NF} = \eta_e G_{BB}$, where G_{BB} is the blackbody thermal conductance, suggesting that the near-field thermal conductance should exhibit less ΔT dependence than the blackbody conductance.

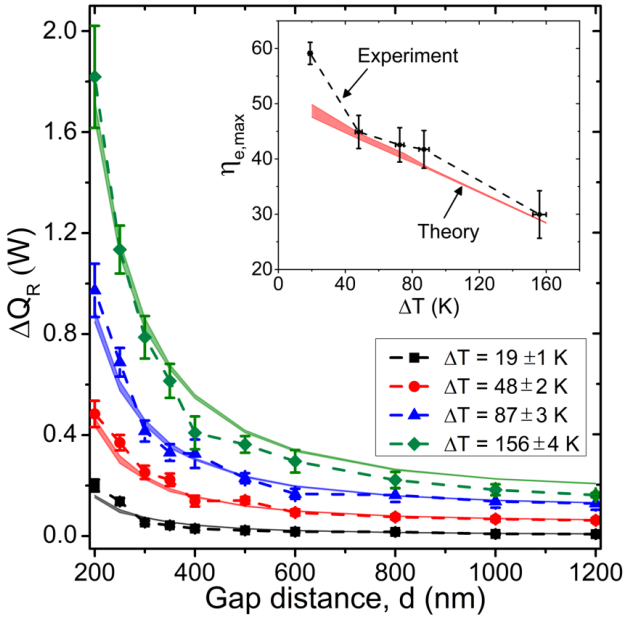

FIG. 4: Gap-dependence of near-field thermal radiation for different thermal gradients. The symbols show the experimental near-field thermal radiative power, where the colored bands are fluctuational electrodynamics predictions. For better presentation of the results, the obtained ΔQ_R curves are slightly offset by 0.05 W. The inset shows the Maximum enhancement factor ($\eta_{e,max}$) at the gap distance of 200 nm.

In addition to the gap distance and temperature gradient, the degree of parallelism between two planes is another critical factor in the accurate measurement of plane-plane near-field thermal radiation. In order to demonstrate the significance of parallelism, we measured near-field thermal radiation while tilting the nanopositioning stage from the initially aligned parallel position. Figure 5 shows the change of ΔQ_R as a function of θ_x (i.e., the angle of the bottom plate about the $x-$axis) when $T_H = 319.5 \pm 0.5$ K and $T_C = 300.5 \pm 0.5$ K at the gap distance of 400 nm. The obtained results reveal that even a small deviation from the parallel position can result in noticeable decrease of the radiative heat transfer rate: ΔQ_R changes by ∼±5% when the bottom stage is tilted by around $\pm2 \times 10^{-3}$ deg. The same trend can be observed when θ_y is manipulated: see Fig. S9 [44]. This high sensitivity to the tilted angle can be effectively used as an alternative parallelism control scheme between large planar structures by conducting the angular alignment to make the maximum near-field thermal radiation.

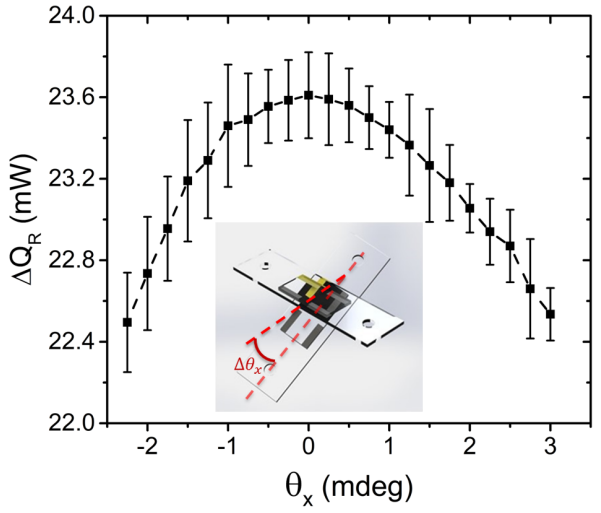

FIG. 5: Effect of parallelism on near-field thermal radiation, ΔQ_R, as a function of θ_x when $\theta_y = 0$ deg. The thermal gradient is set to $\Delta T = 19\pm1$ K (i.e., $T_H = 319.5\pm0.5$ K and $T_C = 300.5\pm0.5$ K) at the gap distance of 400 nm.

In conclusion, the present work experimentally investigates a near-field enhancement of thermal radiation between macroscale planar structures under a large thermal gradients. We have measured near-field radiative heat transfer between 5×5 mm^2 quartz surfaces for a broad range of temperature gradients from ∼19 K up to ∼156 K. The observed $1/d^2$ gap dependence is in excellent agreement with the fluctuational electrodynamics, demonstrating the strong contribution of surface phonon polaritons to near-field thermal radiation for quartz. We also have measured the sensitivity of the parallelism to near-field thermal radiation. The present work provides solid experimental evidences of super-Planckian energy transfer across a nanoscale vacuum gap, which can directly impact emerging near-field energy applications. In addition, the experimental scheme established in this work will facilitate the measurement of near-field thermal radiation for various materials and structures with the relative easiness in sample preparation and alignment.

We thank Mathieu Francoeur, Rodolphe Vaillon, and Bong Jae Lee for fruitful discussions. This work has been supported by the National Science Foundation (NSF CBET-1403072 and ECCS-1611320). T.K. and N.I. also appreciate the support of the undergraduate research opportunity program (UROP) at the University of Utah.

* Electronic address: kpark@mech.utah.edu

[1] K. Park and Z. M. Zhang, Frontiers in Heat and Mass Transfer **4**, 013001 (2013).
[2] R. S. DiMatteo, P. Greiff, S. L. Finberg, K. A. Young-Waithe, H. K. H. Choy, M. M. Masaki, and C. G. Fonstad, Applied Physics Letters **79**, 1894 (2001).
[3] A. Narayanaswamy and G. Chen, Applied Physics Letters **82**, 3544 (2003).
[4] M. Laroche, R. Carminati, and J.-J. Greffet, Journal of Applied Physics **100**, 063704 (2006).
[5] S. Basu, Y.-B. Chen, and Z. M. Zhang, International Journal of Energy Research **31**, 689 (2007).
[6] O. Ilic, M. Jablan, J. D. Joannopoulos, I. Celanovic, and M. Soljačić, Optics Express **20**, A366 (2012).
[7] K. Chen, P. Santhanam, and S. Fan, Applied Physics Letters **107**, 091106 (2015).
[8] J. K. Tong, W.-C. Hsu, Y. Huang, S. V. Boriskina, and G. Chen, Scientific Reports **5**, 10661 (2015).
[9] M. Ghashami, S. K. Cho, and K. Park, Journal of Quantitative Spectroscopy and Radiative Transfer **198**, 59 (2017).
[10] J. Shi, B. Liu, P. Li, L. Y. Ng, and S. Shen, Nano Letters **15**, 1217 (2015).
[11] C. R. Otey, W. T. Lau, and S. Fan, Physical Review Letters **104**, 154301 (2010).
[12] S. Basu and M. Francoeur, Applied Physics Letters **98**, 113106 (2011).
[13] P. Ben-Abdallah and S.-A. Biehs, Applied Physics Letters **103**, 191907 (2013).
[14] P. Ben-Abdallah and S.-A. Biehs, Physical Review Letters **112**, 044301 (2014).
[15] K. Joulain, Y. Ezzahri, J. Drevillon, B. Rousseau, and D. D. S. Meneses, Optics Express **23**, A1388 (2015).
[16] K. Ito, K. Nishikawa, A. Miura, H. Toshiyoshi, and H. Iizuka, Nano Letters **17**, 4347 (2017).
[17] A. Kittel, W. Müller-Hirsch, J. Parisi, S.-A. Biehs, D. Reddig, and M. Holthaus, Physical Review Letters **95**, 224301 (2005).
[18] K. Kim, B. Song, V. Fernández-Hurtado, W. Lee, W. Jeong, L. Cui, D. Thompson, J. Feist, M. T. Reid, F. J. García-Vidal, et al., Nature **528**, 387 (2015).
[19] K. Kloppstech, N. Könne, S.-A. Biehs, A. W. Rodriguez, L. Worbes, D. Hellmann, and A. Kittel, Nature Communications **8**, 14475 (2017).
[20] L. Cui, W. Jeong, V. Fernández-Hurtado, J. Feist, F. J. García-Vidal, J. C. Cuevas, E. Meyhofer, and P. Reddy, Nature Communications **8**, 14479 (2017).
[21] A. Narayanaswamy, S. Shen, and G. Chen, Physical Review B **78**, 115303 (2008).
[22] E. Rousseau, A. Siria, G. Jourdan, S. Volz, F. Comin, J. Chevrier, and J.-J. Greffet, Nature Photonics **3**, 514 (2009).
[23] S. Shen, A. Narayanaswamy, and G. Chen, Nano Letters **9**, 2909 (2009).
[24] S. Shen, A. Mavrokefalos, P. Sambegoro, and G. Chen, Applied Physics Letters **100**, 233114 (2012).
[25] B. Song, A. Fiorino, E. Meyhofer, and P. Reddy, AIP Advances **5**, 053503 (2015).
[26] P. J. van Zwol, L. Ranno, and J. Chevrier, Physical review letters **108**, 234301 (2012).
[27] P. J. van Zwol, S. Thiele, C. Berger, W. A. de Heer, and J. Chevrier, Physical review letters **109**, 264301 (2012).
[28] B. Song, Y. Ganjeh, S. Sadat, D. Thompson, A. Fiorino, V. Fernández-Hurtado, J. Feist, F. J. Garcia-Vidal, J. C. Cuevas, P. Reddy, et al., Nature Nanotechnology **10**, 253 (2015).
[29] E. G. Cravalho, C. L. Tien, and R. Caren, Journal of Heat Transfer **89**, 351 (1967).
[30] G. Domoto, R. Boehm, and C. L. Tien, Journal of Heat Transfer **92**, 412 (1970).

[31] C. Hargreaves, Physics Letters A **30**, 491 (1969).

[32] L. Hu, A. Narayanaswamy, X. Chen, and G. Chen, Applied Physics Letters **92**, 133106 (2008).

[33] M. Lim, S. S. Lee, and B. J. Lee, Physical Review B **91**, 195136 (2015).

[34] K. Ito, A. Miura, H. Iizuka, and H. Toshiyoshi, Applied Physics Letters **106**, 083504 (2015).

[35] M. P. Bernardi, D. Milovich, and M. Francoeur, Nature Communications **7**, 12900 (2016).

[36] J. I. Watjen, B. Zhao, and Z. M. Zhang, Applied Physics Letters **109**, 203112 (2016).

[37] S. Lang, G. Sharma, S. Molesky, P. Kränzien, T. Jalas, Z. Jacob, A. Y. Petrov, and M. Eich, Scientific Reports **7**, 13916 (2017).

[38] R. St-Gelais, B. Guha, L. Zhu, S. Fan, and M. Lipson, Nano Letters **14**, 6971 (2014).

[39] R. St-Gelais, L. Zhu, S. Fan, and M. Lipson, Nature Nanotechnology **11**, 515 (2016).

[40] R. S. Ottens, V. Quetschke, S. Wise, A. A. Alemi, R. Lundock, G. Mueller, D. H. Reitze, D. B. Tanner, and B. F. Whiting, Physical Review Letters **107**, 014301 (2011).

[41] T. Kralik, P. Hanzelka, V. Musilova, A. Srnka, and M. Zobac, Review of Scientific Instruments **82**, 055106 (2011).

[42] T. Kralik, P. Hanzelka, M. Zobac, V. Musilova, T. Fort, and M. Horak, Physical Review Letters **109**, 224302 (2012).

[43] B. Song, D. Thompson, A. Fiorino, Y. Ganjeh, P. Reddy, and E. Meyhofer, Nature Nanotechnology **11**, 509 (2016).

[44] See Supplemental Material at [URL will be inserted by publisher] for discussions on determination of sample surface temperatures, interferometric calibration of nanopositioner, sample fabrication and preparation, surface characterization, fluctuational electrodynamics model, effect of parallelism between two plates and effect of sample contact to heat transfer, which includes Refs.[45-50].

[45] M. Francoeur and M. P. Mengüç, Journal of Quantitative Spectroscopy and Radiative Transfer **109**, 280 (2008).

[46] M. Francoeur, M. P. Mengüç, and R. Vaillon, Journal of Physics D: Applied Physics **43**, 075501 (2010).

[47] E. D. Palik, *Handbook of Optical Constants of Solids*, vol. 3 (Academic press, 1998).

[48] B. J. Lee, K. Park, T. Walsh, and L. Xu, Journal of solar energy engineering **134**, 021009 (2012).

[49] M. A. Ordal, R. J. Bell, R. W. Alexander, L. L. Long, and M. R. Querry, Applied optics **24**, 4493 (1985).

[50] T. P. Otanicar, P. E. Phelan, R. S. Prasher, G. Rosengarten, and R. A. Taylor, Journal of renewable and sustainable energy **2**, 033102 (2010).

[51] J.-P. Mulet, K. Joulain, R. Carminati, and J.-J. Greffet, Microscale Thermophysical Engineering **6**, 209 (2002).

[52] Y. Ganjeh, B. Song, K. Pagadala, K. Kim, S. Sadat, W. Jeong, K. Kurabayashi, E. Meyhofer, and P. Reddy, Review of Scientific Instruments **83**, 105101 (2012).

[53] D. Polder and M. V. Hove, Physical Review B **4**, 3303 (1971).

[54] S. Rytov, Y. A. Kravtsov, and V. Tatarskii, *Priniciples of Statistical Radiophysics. 3. Elements of Random Fields.* (New York: Springer, 1989).

[55] G. Nellis and S. Klein, *Heat Transfer* (Cambridge University Press, 2009).

[56] J. J. Loomis and H. J. Maris, Physical Review B **50**, 18517 (1994).

[57] S.-A. Biehs, E. Rousseau, and J.-J. Greffet, Physical review letters **105**, 234301 (2010).

[58] K. Joulain, J.-P. Mulet, F. Marquier, R. Carminati, and J.-J. Greffet, Surface Science Reports **57**, 59 (2005).

[59] A. Volokitin and B. N. Persson, Reviews of Modern Physics **79**, 1291 (2007).

[60] M. Francoeur, R. Vaillon, and M. P. Mengüç, Energy Conversion, IEEE Transactions on **26**, 686 (2011).